Kondo transport through a quantum dot coupled with side quantum-dot structures*

Jiang Zhao-Tan(江兆潭)†

[a] Department of Physics, Beijing Institute of Technology, Beijing 100081, China
[b] Department of Physics, Oklahoma State University, Stillwater, Oklahoma 74078, USA

(Received 7 January 2010; revised manuscript received 27 January 2010)

This paper investigates Kondo transport properties in a quadruple quantum dot (QD) based on the slave-boson mean field theory and the non-equilibrium Green's function. In the quadruple QD structure one Kondo-type QD sandwiched between two leads is side coupled to two separate QD structures: a single-QD atom and a double-QD molecule. It shows that the conductance valleys and peaks always appear in pairs and by tuning the energy levels in three side QDs, the one-, two-, or three-valley conductance pattern can be obtained. Furthermore, it finds that whether the valley and the peak can appear is closely dependent on the specific values of the interdot couplings and the energy level difference between the two QDs in the molecule. More interestingly, an extra novel conductance peak can be produced by the coexistence of the two different kinds of side QD structures.

Keywords: quantum transport, Kondo effect, quantum dot
PACC: 7335C

1. Introduction

The Kondo effect,[1] as a typical many-body correlated phenomenon, has attracted considerable theoretical and experimental attention. Owing to the rapid advances in the low-temperature and semiconductor-fabricating technologies, extensive studies on Kondo effects have also been carried out in artificial atomic or molecular quantum-dot (QD) structures.[2−14] In recent years, based on the single-QD or double-QD structure, many interesting subjects, such as the single-impurity Kondo effect, the double-impurity Kondo effect, many-channel Kondo effect, and the competition between Kondo effect and anti-ferromagnetic interaction or Ruderman–Kittel–Kasuya–Yosida (RKKY) interaction, have been investigated.[15−17] On the other hand, different kinds of QD structures have been proposed according to the specific research objectives. In general, QD structures[18−26] can be classified into four kinds: serially coupled QDs, horizontally coupled QDs, circularly coupled QDs, and side-coupled QDs. Just very recently, people start to consider the side-coupled QDs theoretically and experimentally.[27−31]

First Güclü *et al.*[32] studied the transport properties in a setup with a noninteracting QD and a side Kondo-type QD. Then using a strongly correlated QD attached to two leads with a side noninteracting QD, Wu *et al.*[33] studied the transport properties and the influences of the side single QD. It is demonstrated that the linear conductance will depart from the unitary limit due to the interdot coupling. Moreover, Tanamoto and Nishi devised a similar setup with a side-coupled double-QD structure to study the Fano–Kondo effect.[34] Afterwards, Trocha and Barnaś investigated the Kondo–Dicke resonances in the electron transport through a triple QD system with two separate side QDs.[35] These studies may be viewed as the starting point of the studies on the QD system with side-coupled QD structures.

Motivated by these researches, in this paper, we propose a new type of quadruple QD setup with two different side-coupled structures: a single-QD atom and a double-QD molecule, as shown in Fig. 1. It should be emphasized that this extension of the side-coupled QD structure is by no means a trivial procedure. As discussed below, studies on this quadruple QD can present much more information which is crucial to help us completely understand the influences on the transport properties caused by the competition between two different side structures. Using the

*Project supported by National Natural Science Foundation of China (Grant Nos. 10604005 and 10974015) and supported by Program for New Century Excellent Talents in University of China (Grant No. NCET-08-0044).
†Corresponding author. E-mail: jiangzhaotan@bit.edu.cn
© 2010 Chinese Physical Society and IOP Publishing Ltd

non-equilibrium Green's function we will study systematically the quantum transport properties in this quadruple QD system. It is shown that the valleys and peaks in the linear conductance curves always appear in pair and one can obtain one-, two-, or three-valley conductance patterns by tuning the energy levels in three side QDs . Whether the valley and the peak can appear is closely dependent on the specific values of the interdot coupling and the energy level difference between the two QDs in the molecule. In addition, the relative position relation between the valley and the peak in each pair is completely determined by the melecular QD energy levels. Moreover, an extra novel conductance peak can be caused by the coexistence of the two different side QD structures.

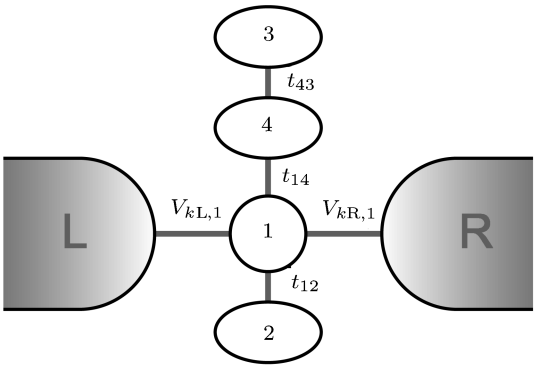


Fig. 1. Schematic illustration of the QD system with two different kinds of side-coupled objects, QD atom (QD2) and molecule (QD3 and QD4), sandwiched between two leads (L and R). The $V_{k\mathrm{L/R},1}$ describes the coupling of QD1 to leads L/R, whereas t_{ij} is the interdot coupling between the ith and the jth QDs with $ij = 12$, 14, 43.

The rest of this article is organized as follows. In Section 2 we give the Hamiltonian of the QD system with the side-coupled three QDs and the derivation details of the Green's function and the conductance. In Section 3 the numerical results and discussion are presented. Finally, a conclusion is outlined in Section 4.

2. Model and formulation

We consider a complex system composed of four single-level QDs, one small QD1 and three large QDs 2, 3, and 4, sandwiched between the left (L) and right (R) leads (see Fig. 1). The entire system under consideration can be modeled by the Anderson impurity Hamiltonian $H = H_{\mathrm{dot}} + H_{\mathrm{leads}} + H_{\mathrm{coup}}$, in which the first term describes the Hamiltonian of the four QD system

$$H_{\mathrm{dot}} = \sum_{i\sigma}\left(\varepsilon_i d^{\dagger}_{i\sigma} d_{i\sigma} + U_i d^{\dagger}_{i\sigma} d_{i\sigma} d^{\dagger}_{i\bar{\sigma}} d_{i\bar{\sigma}}/2\right) + \sum_{\langle ij\rangle,\sigma}\left(t_{ij} d^{\dagger}_{i\sigma} d_{j\sigma} + h.c.\right). \quad (1)$$

Here ε_i ($i = 1$, 2, 3, 4) denotes the ground-state energy of the ith QD and U_i the corresponding intradot Coulomb repulsion interaction. The $d^{\dagger}_{i\sigma}$ ($d_{i\sigma}$) is the creation (annihilation) operator of the electron in the state ε_i and t_{ij} represents the interdot coupling between the ith and jth QDs with $\langle ij\rangle = 12$, 14, 34. The noninteracting electrons in the left and right leads are modeled by

$$H_{\mathrm{leads}} = \sum_{k\sigma\alpha=\mathrm{L,R}} \varepsilon_{k\alpha} c^{\dagger}_{k\sigma\alpha} c_{k\sigma\alpha} \quad (2)$$

with $\varepsilon_{k\sigma\alpha}$ being the energy of an electron with wave vector k and spin σ in the αth lead, and $c^{\dagger}_{k\sigma\alpha}(c_{k\sigma\alpha})$ the corresponding creation (annihilation) operator. The coupling between the two leads and QD1 is denoted by

$$H_{\mathrm{coup}} = \sum_{k\sigma\alpha} V_{k\alpha,1} c^{\dagger}_{k\sigma\alpha} d_{1\sigma} + \mathrm{h.c.}, \quad (3)$$

where $V_{k\alpha,1}$ represents the hopping term between the αth lead and QD1.

In the regime here we consider that the Coulomb interactions $U_{2,3,4}$ in QDs 2,3,4 are kept to be 0, and the Coulomb interaction U_1 in QD1 is chosen to be ∞, which forbids the double occupancy on QD1. Thus we can make use of the infinite-U slave-boson mean-field (SBMF) approach to discuss its Kondo transport properties. Therefore, in the auxiliary slave-boson representation the Anderson Hamiltonian H can be reexpressed as[36]

$$\mathcal{H} = \sum_{k\sigma\alpha} \varepsilon_{k\sigma\alpha} c^{\dagger}_{k\sigma\alpha} c_{k\sigma\alpha} + \sum_{\sigma} \tilde{\varepsilon}_1 f^{\dagger}_{1\sigma} f_{1\sigma} + \sum_{p\sigma} \varepsilon_p d^{\dagger}_{p\sigma} d_{p\sigma} + \sum_{\sigma}(t_{43} d^{\dagger}_{4\sigma} d_{3\sigma} + t_{12} f^{\dagger}_{1\sigma} b d_{2\sigma} + t_{14} f^{\dagger}_{1\sigma} b d_{4\sigma} + \mathrm{h.c.}) + \sum_{k\sigma\alpha}(V_{k\alpha,1} c^{\dagger}_{k\sigma\alpha} b^{\dagger} f_{1\sigma} + \mathrm{h.c.}) + \lambda(b^{\dagger} b - 1). \quad (4)$$

To derive the above Hamiltonian the creation (annihilation) operator $d^{\dagger}_{1\sigma}$ ($d_{1\sigma}$) is decomposed into $f^{\dagger}_{1\sigma} b$ ($b^{\dagger} f_{1\sigma}$) and the constraint $b^{\dagger} b + \sum_{\sigma} f^{\dagger}_{1\sigma} f_{1\sigma} = 1$ is also taken into account by a Lagrange multiplier λ. Based on the slave-boson mean field approximations the operators $b^{\dagger}$ and b are replaced by a constant c number b, indicating that the charge fluctuations around the average $\langle b(t)\rangle$ are ignored. The two undermined parameters b and λ can be determined by the following

self-consistent equations

$$b^2 - \mathrm{i}\sum_\sigma \int \frac{\mathrm{d}\varepsilon}{2\pi} G^<_{11\sigma}(\varepsilon) = 1, \tag{5}$$

$$\lambda b^2 = \mathrm{i}\sum_\sigma \int \frac{\mathrm{d}\varepsilon}{2\pi} (\varepsilon - \tilde{\varepsilon}_1) G^<_{11\sigma}(\varepsilon). \tag{6}$$

Here $G^<_{11\sigma}(\varepsilon)$ is the lesser Green's function, which can be found according to the Dyson equation $G^r = g^r + G^r \Sigma^r g^r$ and the Keldysh equation $G^< = G^r \Sigma^< G^a$.[37−39] Here we show all the required parameters used in the Dyson and Keldysh equations. The retarded Green's functions of the isolated QDs can be expressed in the 4×4 matrix form with the diagonal elements $g^r_{11} = (\varepsilon - \tilde{\varepsilon}_1 + \mathrm{i}\,0^+)^{-1}$ and $g^r_{pp} = (\varepsilon - \varepsilon_p + \mathrm{i}\,0^+)^{-1}$ for $p = 2, 3, 4$ while the non-diagonal ones zero. The lesser self energy can be written as

$$\Sigma^r(\varepsilon) = \begin{pmatrix} -\mathrm{i}\,\tilde{\Gamma}_0, & \tilde{t}_{12}, & 0, & \tilde{t}_{14} \\ \tilde{t}_{21}, & 0, & 0, & 0 \\ 0, & 0, & 0, & t_{34} \\ \tilde{t}_{41}, & 0, & t_{43}, & 0 \end{pmatrix}. \tag{7}$$

Here we define $\tilde{\varepsilon}_1 = \varepsilon_1 + \lambda$, $\tilde{t}_{12} = \tilde{t}_{21} = t_{12}b$, $\tilde{t}_{14} = \tilde{t}_{41} = t_{14}b$, and $\tilde{\Gamma}_0 = (\tilde{\Gamma}_\mathrm{L} + \tilde{\Gamma}_\mathrm{R})/2$. The $\tilde{\Gamma}_\alpha = 2\pi \sum_k \tilde{V}_{k\alpha,1} \tilde{V}^*_{k\alpha,1} \delta(\varepsilon - \varepsilon_{k\alpha})$ is equal to $b^2\Gamma_\alpha$ where $\tilde{V}_{k\alpha,1} = \tilde{V}^*_{k\alpha,1} = bV_{k\alpha,1}$. For the lesser self energy $\Sigma^<$ there is only one non-zero element $\Sigma^<_{11}(\varepsilon) = \mathrm{i}[\tilde{\Gamma}_\mathrm{L} f_\mathrm{L}(\varepsilon) + \tilde{\Gamma}_\mathrm{R} f_\mathrm{R}(\varepsilon)]$. Remarkably, all the parameters in the Dyson or Keldysh equation are 4×4 matrices. The current flowing through the QD system can be expressed by

$$I_\mathrm{R} = \frac{e}{\hbar} \mathrm{Im} \sum_\sigma \int \frac{\mathrm{d}\varepsilon}{2\pi} \tilde{\Gamma}_\mathrm{R} [f_\mathrm{R}(G^r_{11\sigma} - G^a_{11\sigma}) + G^<_{11\sigma}], \tag{8}$$

and the linear conductance is

$$G = \mathrm{d}I_\mathrm{R}/\mathrm{d}V = \frac{e}{\hbar} \mathrm{Im} \sum_\sigma \int \mathrm{d}\varepsilon \tilde{\Gamma}_\mathrm{R} \frac{\mathrm{d}G^<_{11\sigma}}{\mathrm{d}V}. \tag{9}$$

Here the bias is defined as $V = V_\mathrm{L} - V_\mathrm{R}$ with $V_\mathrm{R} = 0$ being the energy zero point and f_R the Fermi distribution function of the right lead. Generally, the current flowing through a two-terminal structure can be expressed as the following typical form $I = (2e/h) \int \mathrm{d}\varepsilon T(\varepsilon)[f_\mathrm{L}(\varepsilon) - f_\mathrm{R}(\varepsilon)]$ with the transmission coefficient $T(\varepsilon)$.[37] For the present model we can obtain its transmission coefficient

$$T(\varepsilon) = \frac{\tilde{\Gamma}_\mathrm{L} \tilde{\Gamma}_\mathrm{R} (A^r_{11})^2}{[(\varepsilon - \tilde{\varepsilon}_1) A^r_{11} + \Delta]^2 + (\tilde{\Gamma}_0 A^r_{11})^2}. \tag{10}$$

Here we introduce two parameters $A^r_{11} \equiv (\varepsilon - \varepsilon_2)[(\varepsilon - \varepsilon_3)(\varepsilon - \varepsilon_4) - |t_{34}|^2])$ and $\Delta \equiv -(\varepsilon - \varepsilon_3)[(\varepsilon - \varepsilon_2)|\tilde{t}_{14}|^2 + (\varepsilon - \varepsilon_4)|\tilde{t}_{12}|^2] + |\tilde{t}_{12}|^2 |t_{34}|^2$. Moreover, in the small-bias limit, the linear conductance can be proved to equal $G(\varepsilon = 0) = 2G_0 T(0)$ with $G_0 \equiv e^2/h$ being conductance unit. Also, we can calculate the local density of states (LDOS) in QD1 according to the formula

$$\rho_1(\varepsilon) = -\mathrm{Im} G^r_{11}/\pi = \frac{2\tilde{\Gamma}_0 (A^r_{11})^2}{\pi\{[(\varepsilon - \tilde{\varepsilon}_1) A^r_{11} + \Delta]^2 + (\tilde{\Gamma}_0 A^r_{11})^2\}}. \tag{11}$$

By comparing Eqs. (10) and (11), we may find that the linear conductance is closely dependent on the LDOS $\rho_1(0)$. Actually, from our results one can easily deduce the formulae for the system with the side-coupled single QD,[32,33] double QDs,[34], or two separate QDs[35] by selecting the suitable parameters, which further manifests the validity of our research. Notably, the model considered here can exhibit much more information than the three systems in Refs. [32]–[35].

3. Results and discussion

Numerical results about the Kondo transport through the quadruple QD system are provided so as to explore the effects on the quantum transport induced by the side-coupled QDs. For convenience we assume the equal tunnel couplings $\Gamma_\mathrm{L} = \Gamma_\mathrm{R} = 1$ as the energy unit, and the bare QD1 energy level $\varepsilon_1 = -3.5$. The low temperature condition with $k_\mathrm{B}T = 10^{-5}$ is kept always throughout the calculation. We here mainly concentrate on the linear conductance near the zero-bias anomaly.

3.1. Effects of QDs' energy levels

In this section we will investigate the influences of the side-coupled QD energy levels on the Kondo transport properties through QD1. To observe all the effects clearly we will discuss the linear conductance in three cases: (i) tuning the energy level ε_2 of QD2 only; (ii) tuning the energy levels ε_3 and ε_4 of QDs 3 and 4 simultaneously; and (iii) tuning all three energy levels $\varepsilon_2 = \varepsilon_3 = \varepsilon_4$.

In Fig. 2 we first consider the influence of the QD2 energy level on the linear conductance $G(0)$. Figure 2(a) shows the conductance curves when ε_3=ε_4=−0.2 is smaller than $\tilde{\varepsilon}_1 \approx V_\mathrm{L}$=$V_\mathrm{R}$=0. In the case of t_{12}=0.01, QD2 is weakly coupled to QD1 and inclined to decouple from QD1 in the region of $|\varepsilon_2| >> 0$, where the conductance becomes a constant equal to that of the system only with the QD molecule (QDs

3 and 4). However when $|\varepsilon_2| \approx 0$, close to $\tilde{\varepsilon}_1$, the interdot coupling t_{12} will play a crucial role in renormalizing the LDOS $\rho_1(\varepsilon)$ in QD1, and thus seriously affects the conductance pattern. Especially the LDOS at ε=ε_2=0 is suppressed to be zero, inducing the zero conductance at ε_2=0. On the other hand, the renormalization of $\rho_1(\varepsilon)$ will also induce a resonant conductance peak on the right side of this valley. This means that the side-coupled QD2 can induce an anti-resonance and a resonance in the conductance. As the interdot coupling t_{12} increases, the valley becomes wide, which should be certainly the case since a stronger t_{12} will make the energy level ε_2 mixes strongly with $\tilde{\varepsilon}_1$ in a wider region. However, the bottom of the valley always stays at ε_2=0 while the peak position moves right with the peak becoming wide. Then we study the $G \sim \varepsilon_2$ curves in the other three cases of ε_3=ε_4=0, ε_3=ε_4 >> 0, and even ε_3=0.2 and ε_4=0.1. We can see that there are no qualitative changes occurring in the conductance patterns but some quantitative variations. The appearance of the zero conductance at $\varepsilon_2 = 0$ is due to that the LDOS $\rho_1(\varepsilon)$ of QD1 goes to *zero* at $\varepsilon = \varepsilon_2$, same as the results obtained by Wu *et al.*[33] This property of the *zero* LDOS is immune to the side-coupled QD molecule, which can be seen clearly from Eq. (11).

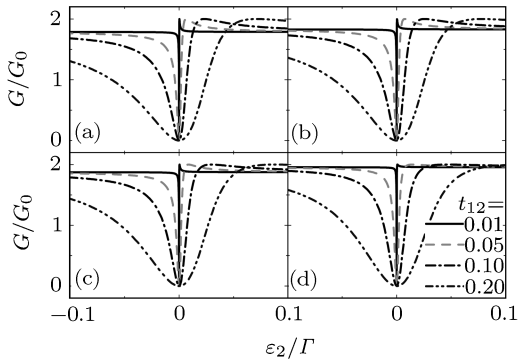


Fig. 2. Conductance as a function of the energy level of QD2 ε_2 for different energy levels (a) $\varepsilon_3 = \varepsilon_4 = -0.2$; (b) 0.0; (c) 0.2; and (d) $\varepsilon_3 = \varepsilon_4 + 0.1 = 0.2$. The interdot couplings are chosen to be $t_{14} = t_{43} = 0.1$.

Next we investigate the second case where the influences of the side-coupled double QDs 3 and 4 are considered by tuning ε_3 and ε_4 while ε_2 is kept invariantly equal to -0.2 or 0.2, respectively in Figs.3(a) or 3(b). For the dashed curve in Fig.3(a) with $\varepsilon_3 = \varepsilon_4$ two anti-resonance valleys can be observed at $\varepsilon_3 = \pm 0.1$, and on the right hand side of each valley a resonance peak is always formed. When $\varepsilon_4 - \varepsilon_3 = \mp 0.1$, the conductances seem to move to right/left relative to that of ε_3= ε_4 with the principal characteristics untouched. Obviously, all these characteristics should be attributed to the side double QDs 3 and 4, which can be understood also from the relation $\rho_1(\varepsilon$=0)=0. It can be easily found that the two anti-resonance positions corresponding to $\rho_1(\varepsilon$=0)=0 are localized at $(-\delta \pm \sqrt{\delta^2 + 4|t_{34}|^2})/2$ with $\delta = \varepsilon_4 - \varepsilon_3$, which give the positions of the conductance valleys. Also we can find a resonance peak on the right side of each valley. Then we examine the curves with $\varepsilon_2 = -0.2$ in Fig. 3(b). We can find that the conductance patterns are very similar to those in Fig. 3(a). It seems that the valley of ε_2 does not affect the conductance pattern at all. In fact, this is not the case. In the cases of $\varepsilon_2 = \pm 0.2$ and the weak interdot couplings ($t_{12} = t_{14} = t_{43}$=0.1), QD2 is almost decoupled from QD1 and thus little effect can be made on the conductance. However, if we choose ε_2 being very close to zero, one can anticipate that serious variations of the conductance patterns will appear. Especially in the limit of ε_2=0 (anti-resonance position), the conductance will always be zero no matter how the energy levels of QD3 and QD4 change. In the same manner, when the side-coupled QDs 3 and 4 are tuned right at the anti-resonance positions, the conductance is also always zero, immune to the side-coupled single QD2.

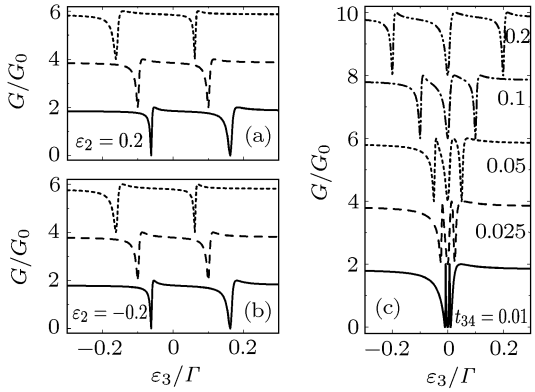


Fig. 3. Conductance G vs the QD3 energy level ε_3 with ε_2=0.2 (a) and -0.2 (b), where the solid, dashed, and dotted curves corresponding to $\varepsilon_4 - \varepsilon_3 = -0.1$, 0.0, and 0.1 are lifted up by 0, 2, and 4, respectively. Here all the interdot couplings are kept to be $t_{12} = t_{14} = t_{43} = 0.1$. For the equal QD energy levels $\varepsilon_2 = \varepsilon_3 = \varepsilon_4$, the conductances are plotted in (c) for the different interdot couplings t_{43}. From bottom to up, the offsets of the curves are selected to be 0, 2, 4, 6, and 8, respectively. Here t_{12} and t_{14} are kept equal to 0.1.

Lastly we study the conductance patterns in Fig. 3(c) when all the three QD levels are kept equal and tuned in the same speed. For the weak interdot coupling t_{34}=0.01 we can see that two sharp peaks

and three narrow valleys are observed. With the increase of t_{34}, the middle valley is always pinned at $\varepsilon_3 = 0$, while the other two valleys at $\pm t_{34}$ move away from each other. Actually the middle valley is determined by the side QD2 and it is reasonable that the valley position is not influenced by the variation of t_{34}. However, the other two valleys induced by the side-coupled double QDs are strongly modified by the interdot coupling t_{34}. This indicates that the interdot coupling between QDs 3 and 4 can seriously change the conductance valley positions. In addition, when t_{34} increases, the sharp peaks between the adjacent valleys in the case of weak t_{34} become broader and eventually evolve into two flats. Also, it should be emphasized that each valley always has an adjoint resonance peak on its right side, indicating that the side QD structures can produce the conductance valley and peak in pair.

3.2. Effects of interdot couplings

In this section, we will turn to study the influences of the interdot coupling t_{34} on the linear conductance. For this purpose, we examine the transmission coefficient again. From the condition $T(\varepsilon{=}0){=}0$ we can find that $\varepsilon_2{=}0$ and $\varepsilon_3\varepsilon_4 = |t_{34}|^2$. Assuming $\varepsilon_4 = \varepsilon_3 + \delta$, the latter condition can be further expressed as $t_{34} = \sqrt{\varepsilon_3(\varepsilon_3+\delta)}$, which gives the zero conductance positions shown in Fig. 4. For a positive (negative) δ, the zero conductance can be established by adjusting t_{34} in the region of $\varepsilon_3 \geq 0$ or $\varepsilon_3 \leq -\delta$ ($\varepsilon_3 \leq 0$ or $\varepsilon_3 \geq -\delta$), called as region I. However, in the region of $-\delta < \varepsilon_3 < 0$ or $0 < \varepsilon_3 < \delta$, called as region II, one can not find such anti-resonance positions any more.

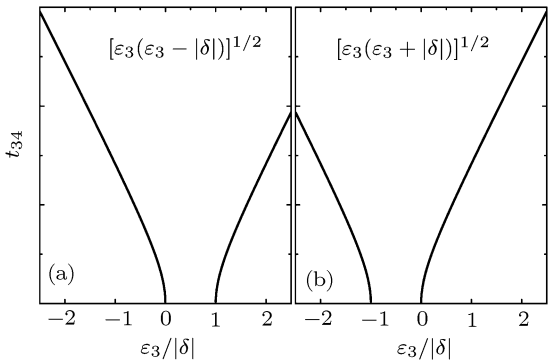


Fig. 4. Variations of the zero conductance positions as a function of ε_3 for $-|\delta|$ (a) and $+|\delta|$ (b).

In the following we will first discuss in Fig. 5 the influences of t_{34} on the transport properties when ε_3 takes the values in region I. For the case of $-|\delta|$ the conductances corresponding to $\varepsilon_2{=}0.1$ and -0.1 are shown in Figs. 5(a) and 5(b), respectively. When ε_3 takes the value of -0.15 in the region $\varepsilon_3 < 0$, and thus ε_4 is equal to -0.25, we can find an anti-resonance valley at $t_{34} = 0.194$. On the other hand, when ε_3 takes the value of 0.15 (or 0.3) in the region $\varepsilon_3 > -\delta{=}0.1$, a valley can also be found at 0.0866 (or 0.245). Notably, there exists a resonance peak localized on the right side of the valley when $\varepsilon_3 < 0$ while on the left side when $\varepsilon_3 > -\delta$. This is also the case for $\varepsilon_2 = -0.1$ shown in Fig. 5(b). Now we turn to examine the transport properties with $\delta = 0.1$ in Figs. 5(c) and 5(d). Obviously in the region of $\varepsilon_3 < -\delta = -0.1$ there exists a conductance valley with a resonance peak on its right side. However, a resonance peak will be found on the left side of the valley for $\varepsilon_3 > 0$. These results indicate that the interdot coupling t_{34} between QDs 3 and 4 can induce an anti-resonance valley and a resonance peak for a certain QDs energy level configuration. To summarize, when ε_3 is in the left part of region I, the conductance peak is localized on the right side of the valley while it is on the left side when ε_3 is in the right part of region I.

Finally, we explore the conductance when ε_3 is localized in region II. For convenience we re-express the transmission coefficient in Eq. (10) as $T(\varepsilon=0) = \tilde{\Gamma}_0^2/([\tilde{\varepsilon}_1 - \Delta(0)/A_{11}^r(0)]^2 + \tilde{\Gamma}_0^2)$ with $\tilde{\Gamma}_{\rm L} = \tilde{\Gamma}_{\rm R} = \tilde{\Gamma}_0$. Generally $\tilde{\varepsilon}_1$ is pinned at the Fermi energy (≈ 0) and hence the transmission coefficient is mainly determined by the term $-\Delta(0)/A_{11}^r(0) \equiv \gamma$. When $|\gamma|$ is equal to 0 (∞), the transmission coefficient approaches 1 (0). For simplicity, by choosing $t_{12} = t_{14} = t_0$ we obtain a concise formula $\gamma = -\tilde{t}_0^2\left[1/\varepsilon_2 + 1/(\varepsilon_4 - t_{34}^2/\varepsilon_3)\right]$. For the case in Fig. 4(a), when ε_3 takes the values from 0 to $|\delta|$, ε_4 takes the values from $-|\delta|$ to 0. In the limit of $\varepsilon_3 \to 0^+$ and $\varepsilon_4 \to -|\delta|$ we obtain $\gamma = -\tilde{t}_0^2/\varepsilon_2$. The conductance becomes independent of t_{34} as shown by the solid curve in Fig. 5(a). When ε_2 approaches zero, the transmission coefficient approaches 0 because $|\gamma| \to \infty$, in agreement with the discussion in Subsection 3.2. In the other limit of $\varepsilon_3 \to |\delta|$ and $\varepsilon_4 \to 0^-$, we have $\gamma = -\tilde{t}_0^2(1/\varepsilon_2 - |\delta|/t_{34}^2)$. As t_{34} increases from zero, γ will decrease from $+\infty$ and thus the conductance increases from zero, see the dash-dotted curve in Fig. 5(b). For a general $\varepsilon_2 \neq 0$, only when QD3 is decoupled from QD4 with $|\delta| \to \infty$ or $t_{34} \to 0$, the conductance approaches zero in the case of $\varepsilon_4 = 0$. This verifies that for the quadruple QD system con-

sidered here the anti-resonance valley does not exist in region II when $\varepsilon_2 \neq 0$. Furthermore we consider the resonance conductance peaks. Note that for certain value of $1/(\varepsilon_4 - t_{34}^2/\varepsilon_3)$, $T(0) = 1$ can be relatively easier to be established by adjusting the parameter ε_2 since ε_2 is independent of $\varepsilon_{3,4}$. It should be emphasized that this is a new type of resonance caused by both side QD structures. Similar results can be obtained by analysing the case shown in Fig. 4(b).

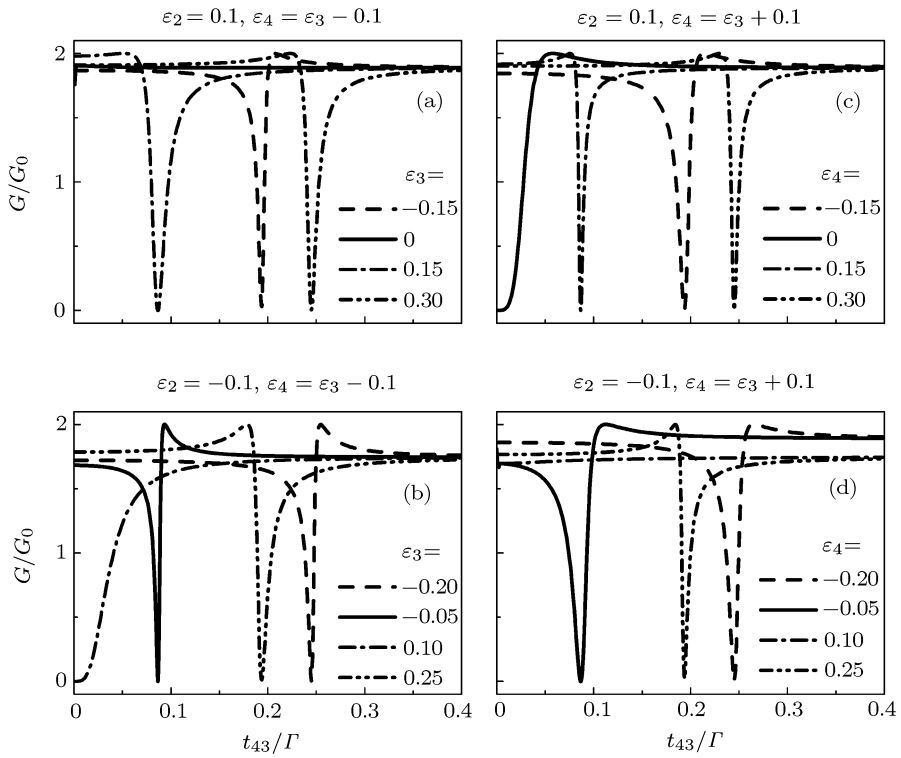


Fig. 5. Variation of the conductance as a function of t_{43} while the other two interdot couplings are kept to be $t_{12} = t_{14} = 0.1$ for the different QD energy level configurations.

4. Conclusion

In conclusion, we investigate the transport properties through the quadruple QD system. We mainly concentrate on the influences on the linear conductance induced by two different kinds of side structures. It is found that by tuning the energy levels in three side QDs one can observe one-, two-, or three-valley conductance patterns. Furthermore, the conductance valleys and peaks appear always in pairs and their appearance is closely dependent on the specific values of the interdot coupling and the energy level difference between the two QDs in the molecule. Also, an extra novel conductance peak can be produced by the coexistence of the two different kinds of side QD structures.

Acknowledgments

The author would like to thank Professor Xin-Cheng Xie (Department of Physics, Oklahoma State University, USA) for the hospitality and the financial support. Also, the author would like to thank Ms. Yan-Nan Yang (Department of the Physics, Beijing Institute of Technology, China) for the valuable discussion.

References

[1] Kondo J 1964 *Prog. Theor. Phys.* **32** 37

[2] Ng T K and Lee P A 1988 *Phys. Rev. Lett.* **61** 1768

[3] Goldhaber-Gordon D, Shtrikman H, Mahalu D, Abusch-Magder D, Meirav U and Kastner M A 1998 *Nature* **391** 156.

[4] Cronenwett S M, Oosterkamp T H and Kouwenhoven L P 1998 *Science* **281** 540

[5] Van der Wiel W G, Franceschi S D, Fujisawa T, Elzerman J M, Tarucha S and Kouwenhoven L P 2000 *Science* **289** 2105

[6] Sasaki S, Franceschi S D, Elzerman J M, van Der Wiel W G, Eto M, Tarucha S and Kouwenhoven L P 2000 *Nature* **405** 764

[7] Ji Y, Heiblum M, Sprinzak D, Mahalu D and Shtrikman H 2000 *Science* **290** 779

[8] Nordlander P, Pustilnik M, Meir Y, Wingreen N S and Langreth D C 1999 *Phys. Rev. Lett.* **83** 808

[9] Zhang P, Xue Q K, Wang Y and Xie X C 2002 *Phys. Rev. Lett.* **89** 286803

[10] Luo H G, Xiang T, Wang X Q, Su Z B and Yu L 2004 *Phys. Rev. Lett.* **92** 256602

[11] Hu H, Zhang G M and Yu L 2001 *Phys. Rev. Lett.* **86** 5558

[12] Sun Q F, Guo H and Lin T H 2001 *Phys. Rev. Lett.* **87** 176601

[13] Jayaprakash C, Krishna-murthy H R and Wilkins J W 1981 *Phys. Rev. Lett.* **47** 737

[14] Jones B A, Varma C M and Wilkins J W 1988 *Phys. Rev. Lett.* **61** 125

[15] Jeong H, Chang A M and Melloch M R 2001 *Science* **293** 2221

[16] Craig N J, Taylor J M, Lester E A, Marcus C M, Hanson M P and Gossard A C 2004 *Science* **304** 565

[17] Vavilov M G and Glazman L I 2005 *Phys. Rev. Lett.* **94** 086805

[18] Simon P, López R and Oreg Y 2005 *Phys. Rev. Lett.* **92** 086602

[19] Chen M L and Wang S J 2007 *Chin. Phys.* **16** 2096

[20] Wu S Q, He Z, Yan C H, Chen X W and Sun W L 2006 *Acta Phys. Sin.* **55** 1413

[21] Song H Z, Zhang P, Duan S Q and Zhao X G 2006 *Chin. Phys.* **15** 2130

[22] Dong Q R 2008 *Chin. Phys.* B **17** 1400

[23] Yin J W, Xiao J L, Yu Y F and Wang Z W 2009 *Chin. Phys.* B **18** 446

[24] Hou T, Wu S Q, Bi A H, Yang F B, Chen J F and Fan M 2009 *Chin. Phys.* B **18** 783

[25] Sun K W and Xiong S J 2006 *Chin. Phys.* **15** 828

[26] Li S S and Xia J B 2007 *Chin. Phys.* **16** 1

[27] Jiang Z T, You J Q, Bian S B and Zheng H Z, 2002 *Phys. Rev.* B **66** 205306

[28] Jiang Z T and Sun Q F, 2007 *J. Phys.: Condens. Matter* **19** 156213

[29] Kang K, Cho S Y, Kim J J and Shin S C 2001 *Phys. Rev.* B **63** 113304

[30] Torio M E, Hallberg K, Ceccatto A H and Proetto C R 2002 *Phys. Rev.* B **65** 085302

[31] Orellana P A, Domníguez-Adame F, Góez I and Ladróde Guevara M L 2003 *Phys. Rev.* B **67** 085321

[32] Kobayashi K, Aikawa H, Sano A, Katsumoto S and Iye Y 2004 *Phys. Rev.* B **70** 035319

[33] Sato M, Aikawa H, Kobayashi K, Katsumoto S and Iye Y 2005 *Phys. Rev. Lett.* **95** 066801

[34] Güçlü A D, Sun Q F and Guo H 2003 *Phys. Rev.* B **68** 245323

[35] Wu B H, Gao J C and Ahn K H 2005 *Phys. Rev.* B **72** 165313

[36] Tanamoto T and Nishi Y 2007 *Phys. Rev.* B **76** 155319

[37] Trocha P and Barnaś J 2008 *Phys. Rev.* B **78** 075424

[38] Aguado R and Langreth D C 2000 *Phys. Rev. Lett.* **85** 1946

[39] Datta S 2004 *Electronic Transport in Mesoscopic Systems* (Cambridge: Cambridge University Press)

[40] Meir Y and Wingreen N S 1992 *Phys. Rev. Lett.* **68** 2512

[41] Jauho A P, Wingreen N S and Meir Y 1994 *Phys. Rev.* B **50** 5528

[42] Jiang Z T, Sun Q F and Wang Y P 2005 *Phys. Rev.* B **72** 045332

[43] Jiang Z T and Han Q Z 2008 *Phys. Rev.* B **78** 035307